Published in final edited form as:
*IEEE Trans Ultrason Ferroelectr Freq Control*. 2012 January ; 59(1): 50–59. doi:10.1109/TUFFC.2012.2155

# Harmonic Reduction in Capacitive Micromachined Ultrasonic Transducers by Gap Feedback Linearization

**Sarp Satir, IEEE[Student Member]** and **F. Levent Degertekin, IEEE[Senior Member]**

## Abstract

The nonlinear relationship between the electrical input signal and electrostatic force acting on the capacitive micromachined ultrasonic transducer (CMUT) membrane limits its harmonic imaging performance. Several input shaping methods were proposed in order to compensate for the nonlinearity originating from the electrostatic force dependence on the square of the applied voltage. Here we analyze harmonic generation in CMUTs with a time domain model. The model explains the basis of the input shaping methods and suggests that the nonlinearity due to gap dependence of the electrostatic force is also significant. It also suggests that the harmonic distortion in the output pressure can be eliminated by subharmonic AC only excitation of the CMUT in addition to scaling the input voltage with the instantaneous gap. This gap feedback configuration can be approximated by the simple addition of a series impedance to the CMUT capacitance. We analyze several types of series impedance feedback topologies for gap feedback linearization. We show that for subharmonic AC excitation while resistive and capacitive impedances result in a trade-off between input voltage and harmonic distortion for a desired pressure output, harmonic generation can be suppressed while increasing the Pa/V transmit sensitivity for proper series inductance and resistance feedback. We experimentally demonstrate the feedback method by reducing harmonic generation by 10dB for the same output pressure at the fundamental frequency by using a simple series resistor feedback with a CMUT operating at a center frequency of 3 MHz. The proposed methods also allow for utilization of the full CMUT gap for transmit operation and hence should be useful in high intensity ultrasonic applications in addition to harmonic imaging.

### Index Terms

CMUT; harmonic imaging; feedback linearization

## I. INTRODUCTION

Nonlinear harmonic imaging is a recent imaging technique which offers advantages over conventional ultrasound imaging methods. Using the harmonic content in the received echo signals, selective nonlinear images of contrast agents and tissue can be constructed. Harmonic imaging uses narrowband pulses at the fundamental frequency, $f_0$, during transmit and the harmonic content within the received echo signals for image reconstruction. Several methods were proposed to enhance the harmonic information from the received echoes by modifying the transmit signals [1],[2]. Ultrasound images are reconstructed using $2f_0$, or higher order harmonic content of the echo signals, because it offers higher lateral and contrast resolution, with lower side and grating lobes as compared to conventional imaging which utilizes the fundamental frequency $f_0$. Moreover, since the nonlinear waves originate within the field of view, aberration artifacts are reduced due to the one way propagation as compared to two way propagation in conventional imaging [3].

Capacitive micromachined ultrasonic transducers (CMUTs) offer distinct advantages as an alternative to piezoelectric transducers in terms of bandwidth, cost, ease of fabrication, and integration with electronics. The wider bandwidth of the transducer allows for the use the same element as a transmitter at fundamental frequency $f_0$ and as a receiver for higher harmonics. However, CMUTs are nonlinear transducers since the electrostatic force applied to the transducer membrane is a nonlinear function of the input voltage and the instantaneous gap between the electrodes driving the transducer. This nonlinear dependence of the electrostatic force results in collapse phenomenon [4] and distortion of the transmitted ultrasound wave. This CMUT nonlinearity is disadvantageous for harmonic imaging, since the harmonic content of the transmitted signal contributes to the harmonic content in the received signal.

Several input shaping methods have been proposed to reduce the harmonic content in the transmitted signal of CMUTs for harmonic imaging [5],[6],[7]. These methods address the voltage square dependence of the electrostatic force as the source of nonlinearity by modifying the electrical input signal. Novell *et al.* proposed a method of applying additional signals at $f_0$ for linear cancellation or $3f_0$ for nonlinear cancellation of the second harmonic component of the transmitted signal [5].

In this study we show that the addition of a series impedance to the CMUT reduces the total harmonic distortion of the transmitted signal by shaping the input signal applied to the CMUT via instantaneous gap feedback. We first analyzed the nonlinear dynamic behavior of a CMUT using a nonlinear 1D model of the transducer, which we implemented in SIMULINK. Then, different gap feedback topologies were investigated using the model. The cases with a series capacitor, a series resistor, and a series resistor-inductor pair were simulated and results are compared to each other. The relationship between our proposed method and input shaping methods presented in [5] are investigated. Finally the linearization method was implemented experimentally using a CMUT, and results are presented where a 10 dB reduction in second harmonic component is achieved with a simple resistor feedback element.

## II. Nonlinear 1D CMUT Model

We modeled a circular membrane CMUT using a 1D parallel plate capacitor and a circular piston in an infinite rigid baffle. The model is presented in Fig. 1 where $V(t)$ is the acting voltage on the transducer, $i(t)$ is the input current, $m$ and $k$ are the mass and the stiffness of the piston respectively, and $g_0$ is the initial gap. $F_{ES}(t)$ and $F_L(t)$ are total electrostatic and fluid loading acting on the piston respectively, $x(t)$ is the displacement of the piston, and $a$ is the radius of the piston. The governing differential equations that couple the mechanical and electrical domains are:

$$m\ddot{x}(t)+kx(t)=F_{ES}(t)-F_L(t), \tag{1}$$

$$i(t)=\frac{d(C(t)V(t))}{dt}, \tag{2}$$

where $C(t)=\frac{\varepsilon_0\pi a^2}{g(t)}$ is the instantaneous capacitance, $\varepsilon_0$ is the permittivity of free space, and $g(t) = g_0 - x(t)$ is the instantaneous gap of the transducer [8]. Defining the Fourier transform of displacement as $\tilde{x}(\omega)$, the inverse Fourier Transform operator as $\Im^{-1}$, such that $x(t) = \Im^{-1}\{\tilde{x}(\omega)\}$, and the radiation impedance as $\tilde{Z}_R(\omega)$, the electrostatic and fluid loading can be expressed as [4],

$$F_{ES}(t)=\frac{\varepsilon_0\pi a^2}{2}\left(\frac{V(t)}{g(t)}\right)^2, \tag{3}$$

$$F_L(t)=\Im^{-1}\{\tilde{Z}_R(\omega)j\omega\tilde{x}(\omega)\}. \tag{4}$$

For a circular piston, the radiation impedance $\tilde{Z}_R(\omega)$ is given as

$$\tilde{Z}_R(\omega)=\rho_0 c\pi a^2\left(1-\frac{J_1\left(\frac{2a\omega}{c}\right)}{\frac{a\omega}{c}}+\frac{jH_1\left(\frac{2a\omega}{c}\right)}{\frac{a\omega}{c}}\right). \tag{5}$$

Here, $J_1$ is the first order Bessel function, $H_1$ is the Struve function, $\rho_0$ is the density of the immersion medium, and $c$ is speed of sound in the medium [9].

Differential equations (1) and (2) are solved using SIMULINK to simulate average generated surface pressure, $p(t)$, for an arbitrary input signal, $V(t)$, where

$$p(t)=-\frac{F_L(t)}{\pi a^2}. \tag{6}$$

Piston stiffness, $k$, is calculated via finite element analysis using COMSOL by applying a uniform pressure, $P$, over the circular membrane as

$$k=\frac{P\pi a^2}{x_{mean}}, \tag{7}$$

where $x_{mean}$ is the average displacement of the membrane. Piston mass, $m$, is then calculated as

$$m=\frac{k}{(2\pi f_0)^2}. \tag{8}$$

Here, $f_0$ is the first resonance frequency of the membrane in vacuum and is calculated via eigenfrequency analysis in COMSOL [10]. In the scope of this work it is assumed that only the first mode of the membrane is excited when an electrical input signal is applied, and the CMUT membrane is operated in the non-collapsed regime. Other sources of nonlinearity such as inelastic behavior of materials under large deformations are not taken into account.

The SIMULINK model which simulates the transient CMUT behavior for an arbitrary input signal is presented in Fig. 2 where the output of the system is the generated average surface pressure, $p(t)$. In the model, the radiation impedance block, $\tilde{Z}_R(\omega)$, is implemented using an arbitrary finite impulse response filter, which has the frequency response expressed in equation (5). Output pressure, $p(t)$, is then post processed for harmonic analysis.

A CMUT with a 27 MHz center frequency and 55% 3dB fractional bandwidth was designed with dimensions and material properties listed in Table 1 as an example for nonlinear harmonic analysis simulations. The surface pressure on the transducer surface was simulated for a 120V input pulse with a, 3 ns width pulse and 120 V DC bias. The response of the transducer is presented in time and frequency domains in Fig. 3. This transducer is then used

in simulations to investigate the nonlinearity in the case of harmonic imaging with $f_0$=20MHz, fundamental transmit, and $2f_0$=40MHz, harmonic receive operation.

## III. Nonlinearity Analysis

Equations (1)–(3) show that the nonlinear behavior of the CMUT is due to the dependency of the electrostatic force on the electrical input signal and instantaneous gap such that

$$F_{ES}(t) \propto V(t)^2, \quad F_{ES}(t) \propto \frac{1}{g(t)^2}. \tag{9}$$

Usually the CMUT is directly driven with a voltage $V(t)$ that includes DC and AC components, i.e. $V(t)=V_{DC}+V_{AC}\cos(\omega t)$. The square of this signal given in (10) has a second harmonic content.

$$V(t)^2=V_{DC}^2+2V_{DC}V_{AC}\cos(\omega t)+(V_{AC}\cos(\omega t))^2, \quad V(t)^2=\frac{V_{AC}^2}{2}+V_{DC}^2+2V_{DC}V_{AC}\cos(\omega t)+\frac{V_{AC}^2}{2}\cos(2\omega t). \tag{10}$$

This nonlinearity due to the voltage square dependence can be compensated by exciting the transducer with an input signal with frequency $f_0/2$ without DC bias where $f_0$ is the desired fundamental operation frequency. Setting $V_{DC}=0$ V and $\omega=2\pi f_0/2$, Equation (10) yields

$$V(t)^2=\frac{V_{AC}^2}{2}+\frac{V_{AC}^2}{2}\cos(2\pi f_0 t), \tag{11}$$

so that the electrostatic force only has a DC component in addition to a sinusoidal component at the desired frequency, $f_0$.

To have a better understanding of the harmonic generation for different drive schemes, the model is simulated for different stable $V_{DC}$ and $V_{AC}$ combinations. In one case, the membrane is excited at the fundamental frequency, $f_0$ = 20 MHz, where the AC signal is enveloped with a Gaussian curve with a full-width half-maximum of 1 μs. The $f_0$ component and the ratio of 20 MHz to 40 MHz components (harmonic ratio or HR) of the generated surface pressure for the given input signal are presented in Fig. 4. In the other case, the CMUT is driven by a subharmonic signal with no DC bias, i.e. $V(t)=V_{AC}E(t)\cos(2\pi t f_0/2)$, where $E(t)$ is the same Gaussian envelope.

In Fig. 4, it is observed that same output pressure can be achieved at fundamental frequency with different $V_{DC}$–$V_{AC}$ combinations, resulting in different harmonic component amplitudes. In reference [6] it was mentioned that harmonic generation is a function of $V_{DC}$ and $V_{AC}$ such that

$$HR \propto \frac{V_{DC}}{V_{AC}}. \tag{12}$$

Through nonlinear harmonic analysis, the relationship in (12) is verified with simulation results in Fig. 4. For example, ~460kPa pressure at 20 MHz is achieved with either $V_{DC}$ =35V, $V_{AC}$=145V and $V_{DC}$=115V, $V_{AC}$=35V with harmonic ratios of 0 dB and 15 dB respectively. The model is then simulated for subharmonic excitation of the transducer at 10 MHz without DC bias. The output pressure component at 20 MHz is plotted as a function of

the excitation signal amplitude in Fig.5 for $V_{AC}$ values which does not collapse the parallel-plate. In this case, the same pressure, ~460kPa, is achieved with $V_{AC}$=160V with a harmonic ratio of 13 dB, which shows no improvement over the conventional 20 MHz excitation with $V_{DC}$=115V, $V_{AC}$=35V. This observation suggests that subharmonic excitation of the transducer does not compensate for the nonlinear distortion by itself, and the nonlinearity of the transducer is mainly caused by the inverse gap dependence of the electrostatic force.

## IV. Gap Feedback Linearization

According to Equation (3), (1) and (2) can be linearized if the input voltage signal is scaled with the instantaneous gap together with $f_0/2$ excitation without DC bias. Substituting the voltage acting on the transducer $\alpha V_s(t)g(t)$, where $\alpha$ is a constant and $V_s(t)$ is the source voltage, yields

$$F_{ES}(t)=\frac{\varepsilon_0\pi a^2\alpha^2}{2}V_s(t)^2, \tag{13}$$

so the nonlinear behavior due to gap dependence is compensated via nonlinear gap feedback [11]. The remaining nonlinear term $V_S(t)^2$ can be handled by exciting the transducer at half the operating frequency as explained in Section III. The nonlinear feedback topology is presented with the block diagram in Fig. 6. The CMUT subsystem in the diagram is simply the model shown in Fig. 2 where $V(t)$ is the voltage acting on the transducer, $p(t)$ is the pressure output, and $g(t)$ is the instantaneous gap, which is the feedback signal. It is interesting to note that with $f_0/2$ excitation, nonlinear gap feedback generates a $3f_0/2$ component by distorting the input signal. The effect can be seen in Fig. 7, where a 150 $V_{peak}$, 10 MHz, 1 μs FWHM Gaussian enveloped tone burst is applied to the transducer with gap feedback and no DC bias. It is shown that, from the frequency domain perspective, the nonlinear interaction of $f_0/2$ and $3f_0/2$ components in the distorted input signal generate 2 components at $f_0$ and $2f_0$ due to the nonlinear behavior of the transducer. The generated $f_0$ component cancels the second harmonic generation since the electrostatic force is a function of the voltage square. This observation suggests that the nonlinear compensation approach presented by Novell *et al.* [5] can be implemented through gap feedback. Hence, the need for complex input signals and fine calibration of the added third harmonic signal in that approach can be avoided.

In essence, the proposed gap feedback method inherently implements charge control of the transducer, because in this case the charge on the CMUT capacitance is linearly proportional to the input voltage $V_S(t)$,

$$Q(t)=\varepsilon_0\pi a^2\alpha V_s(t), \tag{14}$$

where $\alpha$ is the feedback gain. If the transducer is controlled with a charge driver instead of a voltage source, the electrostatic force acting on the CMUT membrane does not depend on the instantaneous gap either [12].However, charge control implementations in literature are limited to static operation, strictly dependent on the parasitic capacitances in the system and require complex charge driving circuitry [13].

A simple way of scaling the input voltage with instantaneous gap can be realized through the addition of a series, passive electronic component to the CMUT driving circuit as shown in Fig. 8. With the addition of the series impedance, the voltage acting on the transducer becomes

$$V(t)=V_S(t)\frac{g(t)}{g(t)+j\omega Z_S\varepsilon_0\pi a^2}, \tag{15}$$

with harmonic excitation voltage $V_S(t)=V_S e^{j\omega t}$. If $Z_S$ is a function of $g(t)$ such that the denominator of (15) is constant,

$$Z_S(g(t))=\frac{K-g(t)}{j\omega\varepsilon_0\pi a^2}, \tag{16}$$

i.e. $K$ is a constant, the gap feedback can be implemented exactly. If $|j\omega Z_S\varepsilon_0\pi a^2| \gg g(t)$, the voltage acting on the CMUT can be approximated by

$$V(t)\approx V_S(t)\frac{g(t)}{j\omega Z_S\varepsilon_0\pi a^2}, \tag{17}$$

so that the input voltage is scaled with instantaneous gap.

### A. Capacitive Feedback

In an effort to extend the actuation range of parallel plate electrostatic actuators, it was shown that a series capacitor extends the stable region of the CMUT in static operation through gap feedback [12]. With $Z_S=1/j\omega C_S$ for harmonic excitation, the circuit in Fig. 8 is a nonlinear voltage divider. This is because of the fact that the CMUT capacitance, $C(t)$, is a nonlinear function of the voltage across the transducer, where the voltage across the CMUT is

$$V(t)=V_S(t)\frac{g(t)}{g(t)+\frac{\varepsilon_0\pi a^2}{C_S}}. \tag{18}$$

As the input source voltage increases, the instantaneous CMUT gap tends to decrease and this results in a decrease in $V(t)$. This negative feedback effect reduces the nonlinearity and thus stabilizes the transducer for a larger displacement range of the CMUT membrane. However, higher excitation voltages are required as a trade-off for the same membrane displacement because of the voltage division nature of the circuit [12]. The series capacitance value relative to the instantaneous CMUT capacitance determines the voltage division ratio hence the harmonic generation. The approximation of (18) can be written in this case as

$$\begin{aligned} V(t)&\approx V_S(t)\frac{g(t)C_S}{\varepsilon_0\pi a^2}, C_S \ll C(t),\\ V(t)&\approx V_S(t), C_S \gg C(t). \end{aligned} \tag{19}$$

To simulate the system with series impedances, the SIMULINK model is modified to include the passive electrical elements as shown in Fig. 9, Fig. 11 and Fig. 13 for different feedback topologies. In the top part of Fig. 10, the simulated voltage across the transducer normalized to the input voltage is plotted as a function of instantaneous normalized gap. As expected, the relationship between $V(t)$ and $g(t)$ becomes more linear as $C_S$ gets smaller as compared to the initial CMUT capacitance. The bottom graph of Fig. 10 shows that for the same output pressure at the fundamental frequency, one improves the harmonic ratio with feedback. With decreasing $C_S$ values harmonic ratio improves at the expense of increased $V_S$. For the designed transducer, 10 dB reduction in $2f_0$ component is achieved with

$C_s = \frac{\varepsilon_0 \pi a^2}{g_0}$ by doubling the excitation voltage to generate the same pressure output at $f_0$=20 MHz (the dotted curve).

If the series feedback capacitor is designed such that its capacitance changes with CMUT membrane motion, satisfying the relation

$$C_s(g(t)) = \frac{\varepsilon_0 \pi a^2}{K - g(t)}, \tag{20}$$

then the gap feedback can be implemented ideally since the denominator of (18) is constant. This indicates the possibility of an electromechanical device to be used as a variable feedback capacitor to approximate the gap scaling of the input voltage more accurately than the fixed series capacitor case. This observation is worth mentioning; however the variable series capacitor approach is beyond the scope of this paper.

### B. Resistive Feedback

With a resistor used as the feedback component, $Z_S$=$R_S$, the circuit in Fig. 8 is a nonlinear first order low pass filter where the output is $V(t)$. Similar to the capacitive feedback case, the magnitude of the voltage across transducer becomes linearized as a function of CMUT gap as the feedback resistor gets larger. Comparing Fig. 10 and Fig. 12, for the same fundamental and second harmonic pressure amplitudes, the required feedback resistor value can be calculated using the corresponding series capacitance value for the same input signal $V_s(t)$, such that $R_s = \left| \frac{1}{j\omega C_s} \right|$ where ω is the excitation frequency. Due to the low pass filter behavior of the circuit, the required feedback resistor value is inversely proportional to the excitation frequency for the same harmonic reduction. This is because Equation (15) is a function of frequency for $Z_S$=$R_S$. In contrast, capacitive feedback is not dependent on frequency, where nonlinearity is only dependent on the relative value of the feedback capacitor compared to the CMUT capacitance.

### C. RL Feedback

The capacitive nature of the CMUT in the electrical domain can be exploited by connecting a series resistor and a series inductor to the transducer. The resulting circuit becomes a nonlinear second order low pass filter, and the resonant behavior of the resulting electrical circuit can be used to linearize (1) and (2) without the need for increased excitation voltage. A similar method involving a series tuning inductor to stabilize parallel-plate actuators was presented in [14]. With the addition of a series resistor-inductor pair, the differential equation governing the electrical domain of the transducer becomes

$$V_S(t) = R_S\, i(t) + L_S \frac{di(t)}{dt} + \frac{1}{C(t)} \int_0^t i(\tau) d\tau, \tag{21}$$

where the voltage across the transducer generating electrostatic force is

$$V(t) = \frac{1}{C(t)} \int_0^t i(\tau) d\tau. \tag{22}$$

With harmonic excitation signal $V_S(t)$, the nonlinear transfer function between $V_S(t)$ and $V(t)$ becomes

$$V(t)=V_S(t)\frac{g(t)}{g(t)+(j\omega R_S-\omega^2 L_S)\varepsilon_0\pi a^2}. \quad (23)$$

Here the damping ratio and the resonance frequency of the filter is:

$$\omega_0=\frac{1}{\sqrt{L_S C(t)}},\qquad \xi=\frac{R_S}{2}\sqrt{\frac{C(t)}{L_S}}. \quad (24)$$

One needs to select carefully the series resistor and inductor values such that the relationship between *V(t)* and *g(t)* is linearized for *g(t)* in the range from *0* to $g_0$. As presented in the top graph of Fig. 14, if the series inductor is chosen so that the resonance frequency of the circuit is higher than the excitation frequency (indicated by the solid line) the voltage acting on the transducer reduces with increasing gap for most of the range, which is opposite of the desired operation. This results in more nonlinear behavior of the transducer, as the harmonic distortion of the transmitted pressure signal increases for the same excitation signal while the fundamental component remains unchanged. For the other cases in Fig. 14 the constraint of $\omega_0 < \omega$, where ω is the excitation frequency, is satisfied for most of the desired gap range. With that approach the gap-CMUT voltage relationship can be optimized for harmonic distortion and excitation signal amplitude for a given output pressure at the fundamental frequency. The corresponding simulation results in the bottom graph of Fig. 14 show that by using proper RL feedback, the second harmonic component of the generated pressure can be decreased by more than 20 dB without increasing the excitation signal. Moreover, due to the resonant behavior of the circuit, higher output pressure and lower harmonic distortion is achievable for a given excitation signal depending on the damping coefficient of the filter.

## V. Discussion of Simulation Results

Since the collapse phenomenon is related to the nonlinearity of the transducer, feedback linearization and charge control extends the stable displacement region of the CMUT. This has been shown for static operation in [11], [12] and [13]. Here, it is essentially shown that similar techniques can be applied for dynamic operation with different feedback schemes. For example, Fig. 15 plots the output pressure at the fundamental frequency as a function of AC voltage amplitude for one of the L-R feedback cases. In comparison to Fig. 5 which plots the same result for no feedback case, it is seen that not only the relationship between the excitation signal and pressure output at $f_0$ is linearized with gap feedback, but it is possible to increase the transmit sensitivity and the maximum pressure at the fundamental frequency of the transducer.

Note that with any of the series impedance methods the second harmonic levels can be reduced to more than 25dB below the fundamental for a broadband device, making it suitable for harmonic imaging. This is achieved with either reasonably higher voltages in R and C feedback, or with reduced voltage levels with LR feedback, which maybe more difficult to implement in large arrays. Since the stable region of the transducer is extended with gap feedback linearization, the maximum pressure generated at the desired frequency can be increased without collapsing the membrane. Thus, linearization of the CMUT can be useful for high intensity applications like HIFU. The LR feedback case maybe more feasible for HIFU arrays where the channel count is small.

The method is also evaluated for broadband excitation waveforms which are typically used in harmonic imaging. The model is simulated for conventional operation with 2 cycle 20

MHz input signal, subharmonic excitation with and without resistive feedback cases. Note that the input signal is 1 cycle 10 MHz tone burst in subharmonic excitation simulations. Simulation results for generated surface pressure are presented in Fig. 16 in frequency and time domains. As observed, subharmonic excitation does not compensate for the harmonic distortion as we discussed in Section III. With increased input signal amplitude and resistive feedback, ~10 dB reduction in second harmonic is achieved, where higher order harmonics are suppressed more effectively.

An important aspect of the proposed method is that it does not require any changes in the mechanical CMUT design to limit the frequency bandwidth. For applications like harmonic imaging, the gap feedback circuit will be used only for transmission with reduced harmonics so that the bandwidth in receive mode is not affected. Since CMUT design is independent from the linearization method, any generic CMUT can be linearized with the gap feedback method.

A possible implementation of the proposed method in array format would be based on the dual-electrode CMUT structure presented by Guldiken *et al.* in [15] where the transmit and receive electrodes embedded in the transducer membrane are electrically isolated. With the dual-electrode structure, the same element can be used for harmonic imaging by utilizing gap feedback in the transmit path with subharmonic excitation and with no DC bias without any detrimental effect on the separately biased receiver electrode and receiver electronics, or the receiver bandwidth.

## VI. Experimental Results

We conducted initial experiments to demonstrate our method. We chose a CMUT with low collapse voltage and low frequency for these experiments so that our driver amplifier was linear at its output up to the collapse voltage of the CMUT where the response gets highly nonlinear. This ensured that we could explore the whole range of voltage values while the major source of nonlinearity in the measurement was the CMUT behavior as desired. Therefore we fabricated a CMUT with a center frequency of 3 MHz and 133% (1–5MHz) effective fractional bandwidth and with a static collapse voltage of 24 V. Fig. 17 shows the measured pulse echo response of the CMUT and its spectrum when excited with a short pulse. A pair of these transducers is used in a pitch catch configuration for harmonic distortion measurements. The receiver is biased to 22V, close to collapse, for high receive sensitivity. Fig. 18 shows the received pressure spectrum when the transmitting CMUT is excited by a 24 $V_{peak}$ 1.5MHz 15 cycle toneburst for the case without feedback, i.e. direct connection to the amplifier. Note that the excitation is large signal AC at half the desired frequency of 3MHz with no DC bias. In this case, the harmonic signal at 6MHz is 15 dB below the desired 3MHz output. For gap feedback operation, the series resistor approach was used for simplicity. First, the capacitance of the transducer is measured with a network analyzer which is approximately 120 pF and an appropriate resistor, 1kΩ in this case, is connected in series with the amplifier. This sets up a low pass filter with a cut off frequency of 1.5 MHz. With this configuration, where only the transmitter input circuitry is changed, the same output pressure at 3MHz is received with a 40V peak AC signal at 1.5MHz, but the harmonic component at 6MHz is reduced more than 10dB as shown by dashed lines in Fig. 18. In the same figure, the bottom plot shows the simulation results for the same configuration. The results are in good agreement especially given the approximations in the model. This simple experiment effectively demonstrates that a simple gap feedback implementation significantly reduces the harmonic generation of a broadband CMUT with a moderate increase in the applied AC signal level.

## VII. Conclusion

A simple 1D transient model is used to understand the nonlinear behavior of CMUTs. It is shown that subharmonic excitation of CMUTs without DC bias is of limited use for harmonic distortion reduction for high excitation voltage amplitudes. We investigated and compared different gap feedback schemes to reduce harmonic distortion of the CMUT membrane motion and investigated the relationship of our proposed method with linearization methods in the literature. As a summary, the series feedback capacitor improves the harmonic ratio where the operation of the resulting circuit is independent of the frequency and the maximum pressure that can be generated at the fundamental frequency without collapsing the CMUT membrane is increased at the expense of input voltage. It is shown that series resistance utilizing resistive feedback improves the harmonic ratio where the resulting circuit is a first order low pass filter. And the maximum pressure that can be generated, with a trade-off of increased input voltage amplitude similar to the capacitive feedback case, is also improved. A series resistor-inductor pair results in $2^{nd}$ order filter response. With appropriately selected values in this topology, one may achieve the same pressure at the fundamental frequency with lower input voltage. As other feedback configurations, one can also increase the maximum output pressure at the fundamental frequency. Initial experiments we conducted support the findings. Approximately 10 dB improvement in the harmonic ratio is achieved over subharmonic AC only excitation by adding a simple series resistor to a CMUT and increasing the input voltage level, while keeping the magnitude of the fundamental component of the transmit pressure the same.

## Acknowledgments

The authors would like to thank Mr. Jaime Zahorian for fabrication of the CMUTs used in the experiments and for a critical reading of the manuscript. This work is supported by the NIH under the grants HL082811 and EB010070.

## References

1. Shen CC, Wang YC, Hsieh YC. Third Harmonic Transmit Phasing for Tissue Harmonic Generation. IEEE transactions on ultrasonics, ferroelectrics, and frequency control. 2007; Vol. 54:1370–1381.
2. Simpson DH, Chin CT, Burns PN. Pulse Inversion Doppler: A New Method for Detecting Nonlinear Echoes from Microbubble Contrast Agents. IEEE transactions on ultrasonics, ferroelectrics, and frequency control. 1999; Vol. 46:372–382.
3. Szabo, TL. Diagnostic Ultrasound Imaging – Inside Out. Elsevier Academic Press; 2004. Chapter 12.
4. Ladabaum I, Jin X, Soh HT, Atalar A, Khuri-Yakub BT. Surface Micromachined Capacitive Ultrasonic Transducers. IEEE transactions on ultrasonics, ferroelectrics, and frequency control. 1998; Vol. 45:678–690.
5. Novell A, Legros M, Felix N, Bouakaz A. Exploitation of Capacitive Micromachined Transducers for Nonlinear Ultrasound Imaging. IEEE transactions on ultrasonics, ferroelectrics, and frequency control. 2009; Vol. 56:2733–2743.
6. Zhou S, Reynolds P, Hossack J. Precompansated Excitation Waveforms to Suppress Harmonic Generation in MEMS Electrostatic Transducers. IEEE transactions on ultrasonics, ferroelectrics, and frequency control. 2004; Vol. 51:1564–1574.
7. Fraser, JD. Bias Charge Regulator for Capacitive Micromachined Ultrasonic Transducers. U.S. Patent. 6,328,696. 2001 Nov 12.
8. Lohfink A, Eccardt PC. Linear and Nonlinear Equivalent Circuit Modeling of CMUTs. IEEE transactions on ultrasonics, ferroelectrics, and frequency control. 2005; Vol. 52:2163–2172.
9. Kinsler, LE.; Frey, AR.; Coppens, AB.; Sanders, JV. Fundamentals of Acoustics. Wiley; 1999.
10. Senturia, SD. Microsystem Design. Vol. Chapter 6. Springer; 2001.
11. Chu, PB.; Pister, S. Analysis of closed-loop control of parallel-plate electrostatic microgripper; Proceedings of IEEE International Conference on Robotics and Automation; 1994. p. 820-825.

12. Seeger, JI.; Crary, SB. Stabilization of Electrostatically Actuated Mechanical Devices; IEEE International Conference on Solid-State Sensors and Actuators; 1997. p. 1133-1136.

13. Seeger JI, Boser BE. Charge Control of Parallel-Plate, Electrostatic Actuators and the Tip-In Instability. Journal of Microelectromechanical Systems. 2003; Vol. 12:656–671.

14. Kyynäräinen JM, Oja AS, Seppa H. Increasing the Dynamic Range of a Micromechanical Moving-Plate Capacitor. Analog Integrated Circuits and Signal Processing. 2001; Vol. 29:61–70.

15. Guldiken RO, McLean J, Degertekin FL. CMUTs with Dual-Electrode Structure for Improved Transmit and Receive Performance. IEEE transactions on ultrasonics, ferroelectrics, and frequency control. 2006; Vol. 53:483–491.

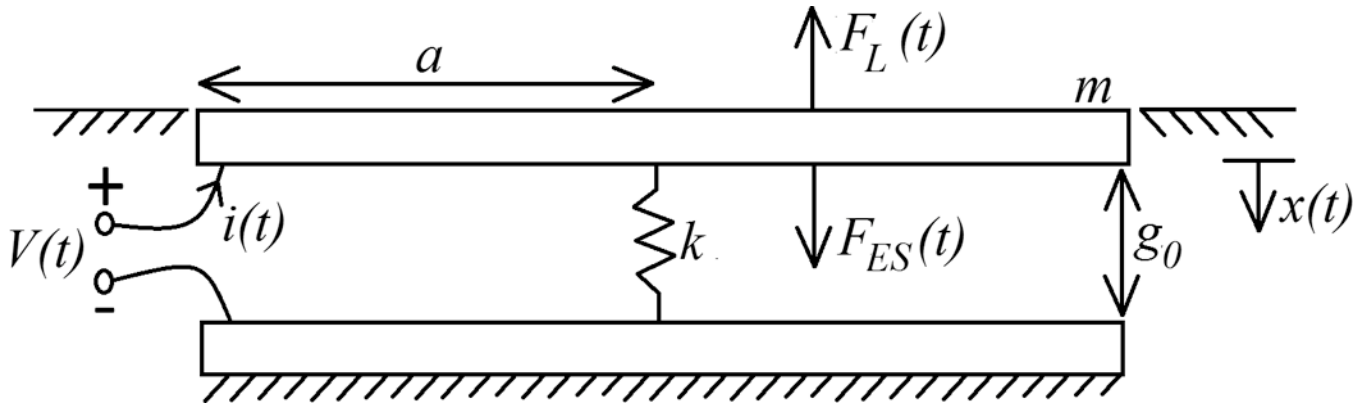


**Fig. 1.**
1D Nonlinear CMUT Model as a parallel plate capacitor and a baffled piston

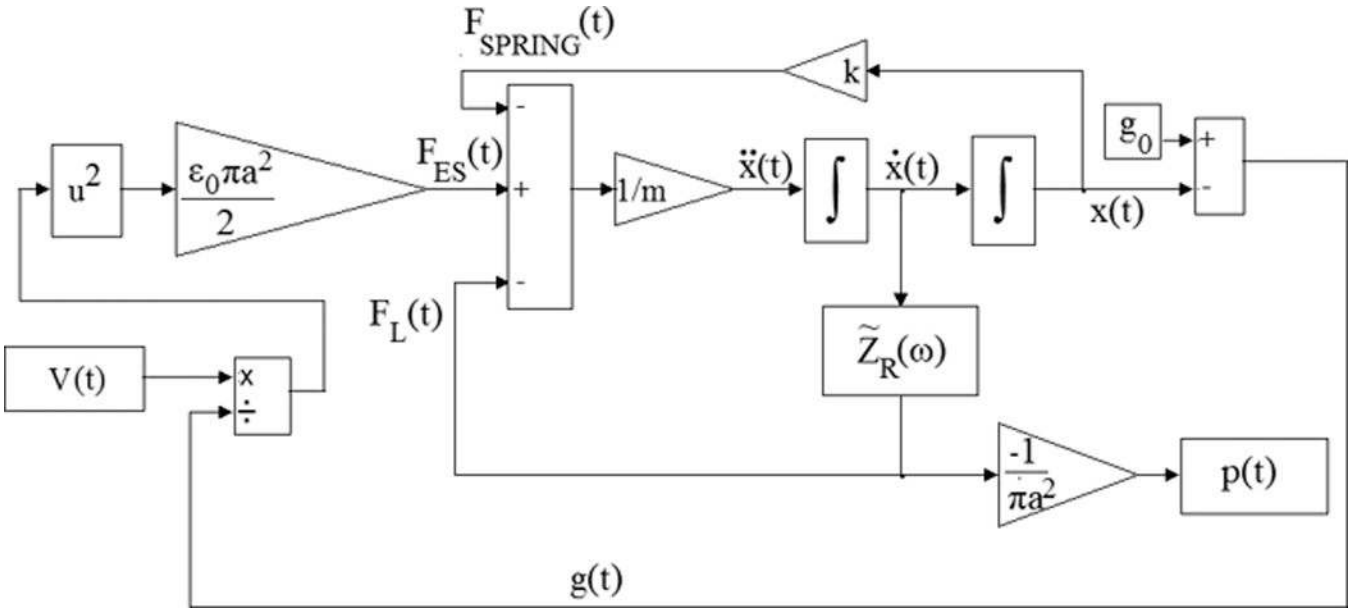


**Fig. 2.**
Nonlinear transient model implemented in SIMULINK for an arbitrary input signal *V(t)* and generated surface pressure *p(t)*

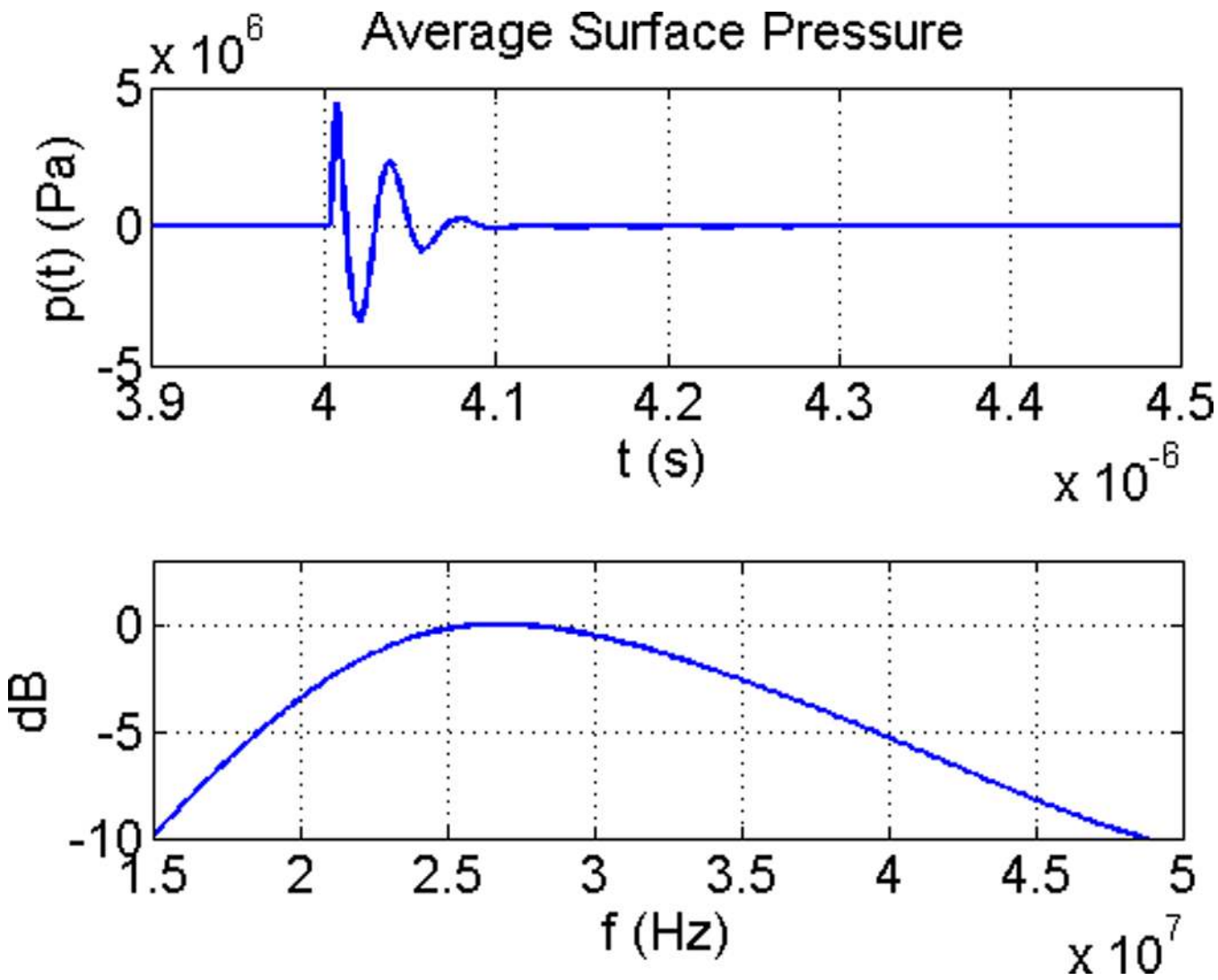


**Fig. 3.**

Simulated impulse response of the CMUT where *V(t)* is a pulse with $V_{DC}$ =120 V, 3ns pulse width and 120 V amplitude and the normalized frequency spectrum of the average surface pressure.

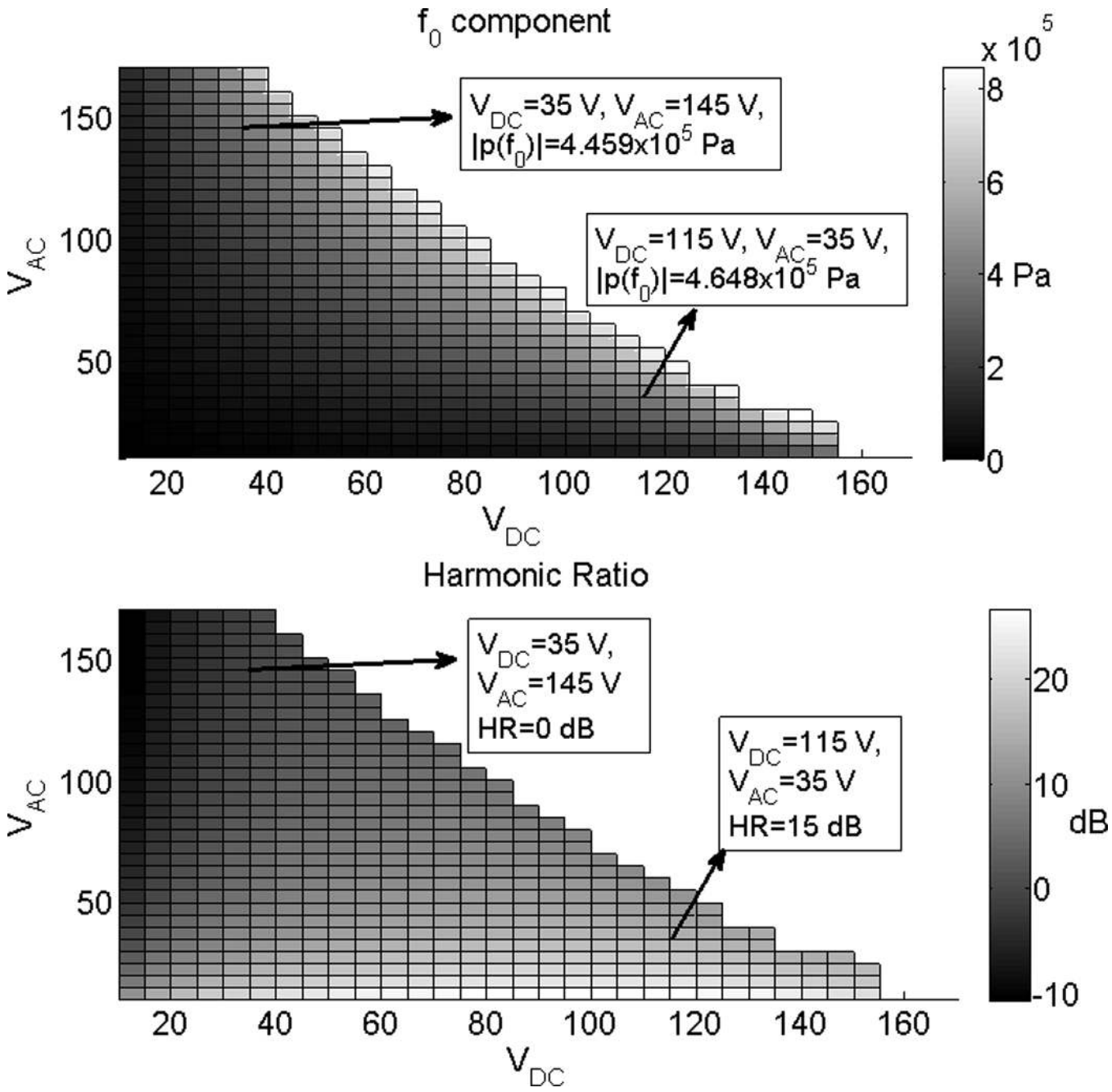


**Fig. 4.**

Magnitude of the $f_0$=20 MHz component and the ratio between 20 MHz and 40 MHz components as a function of $V_{DC}$ and $V_{AC}$. The excitation frequency is 20 MHz.

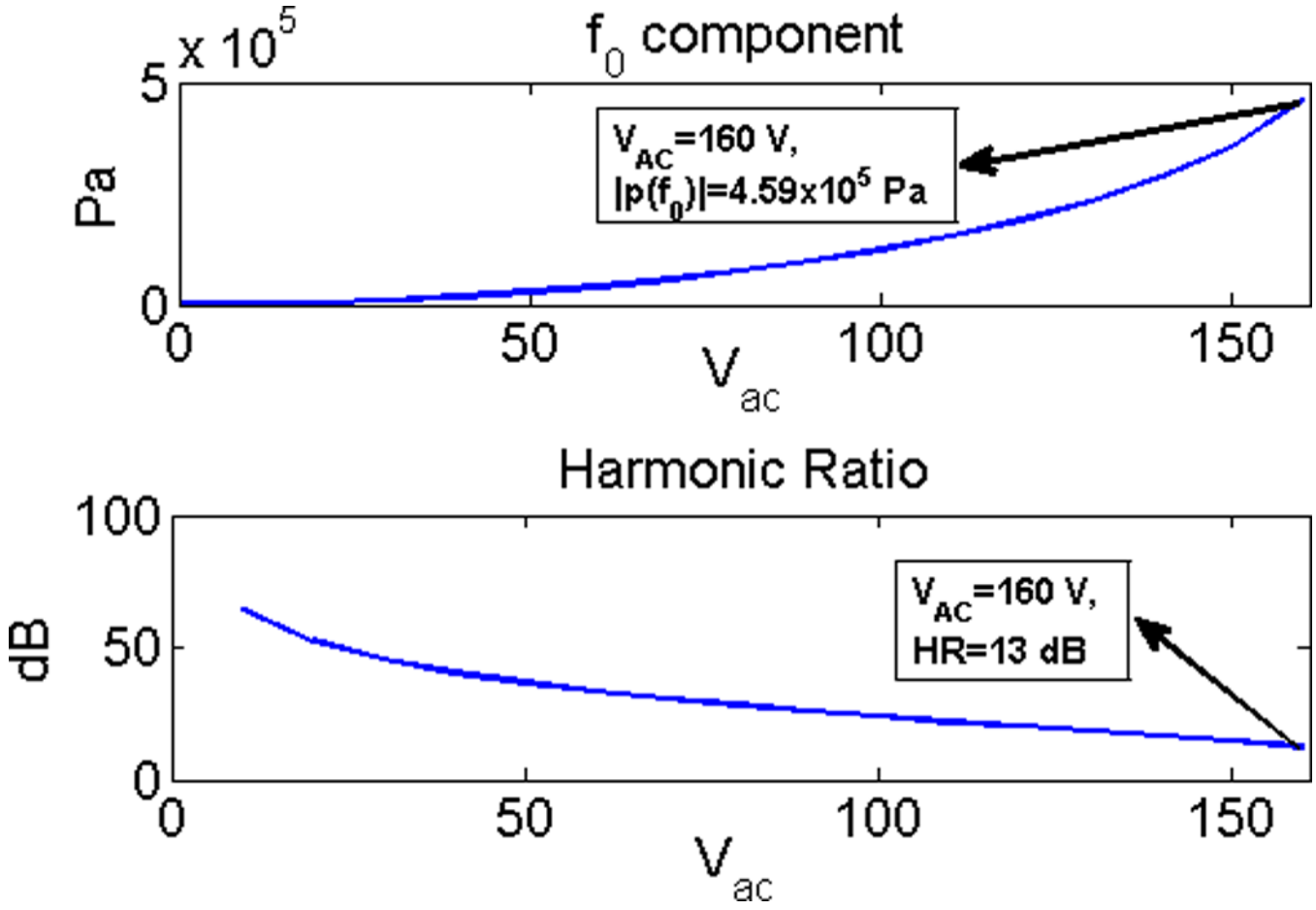


**Fig. 5.**

Magnitude of the $f_0$=20 MHz component and the ratio between 20 MHz and 40 MHz components as a function of $V_{AC}$ with no $V_{DC}$ applied. The excitation frequency is $f_0/2$=10 MHz.

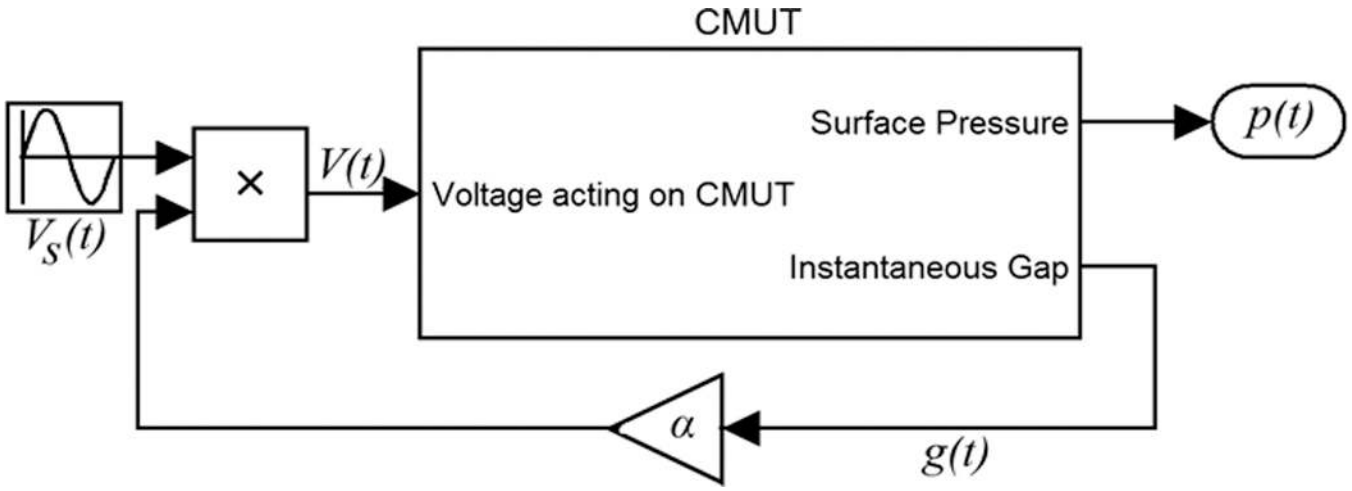


**Fig. 6.**
Block diagram of the nonlinear gap feedback topology

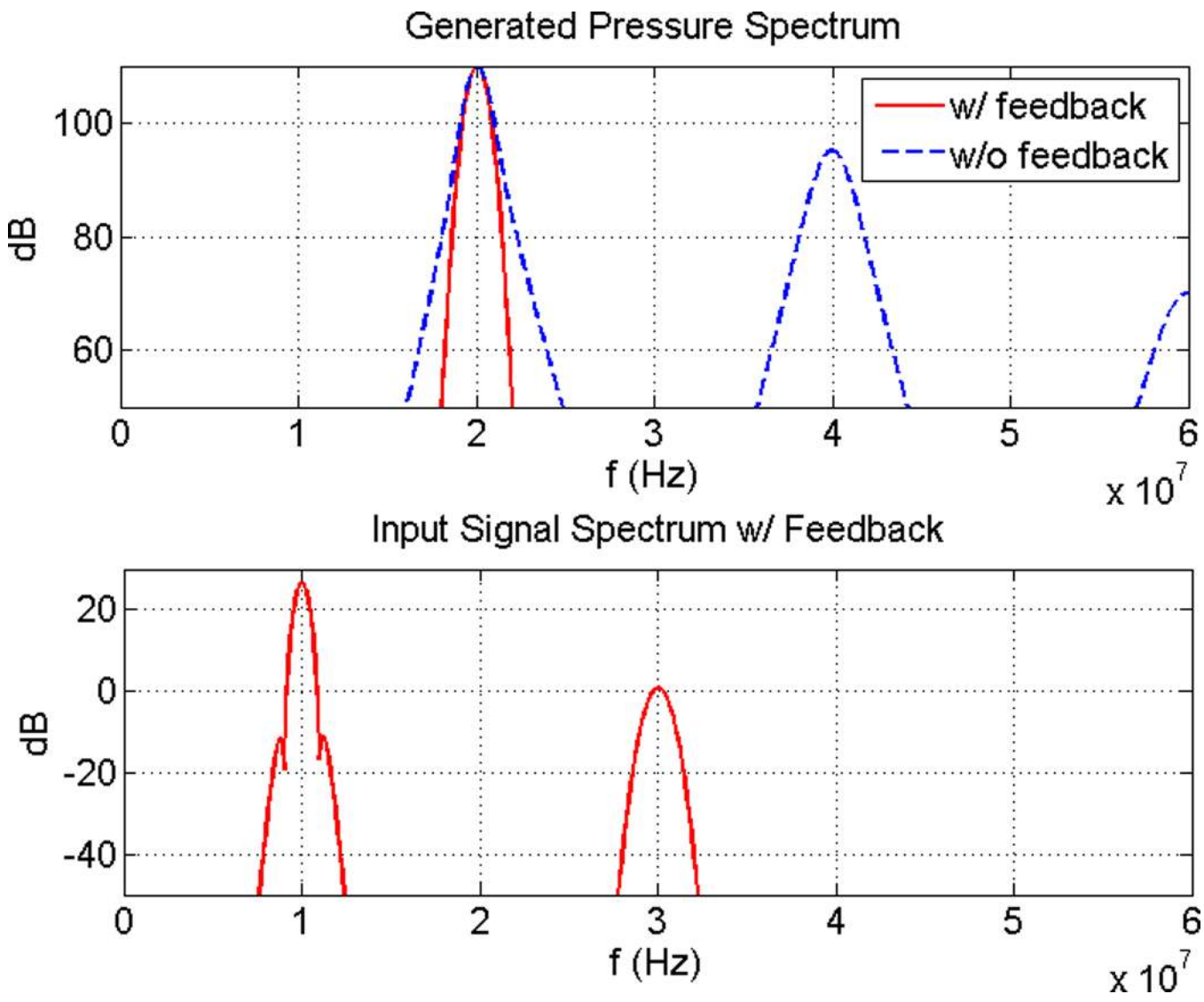


**Fig. 7.**

Top: Magnitude spectrum of generated surface pressure for 10 MHz, 150 $V_{peak}$ excitation signal with and without feedback with corresponding α for the same pressure at 20 MHz. Bottom: The magnitude spectrum of the input voltage, *V(t)*, scaled with instantaneous gap.

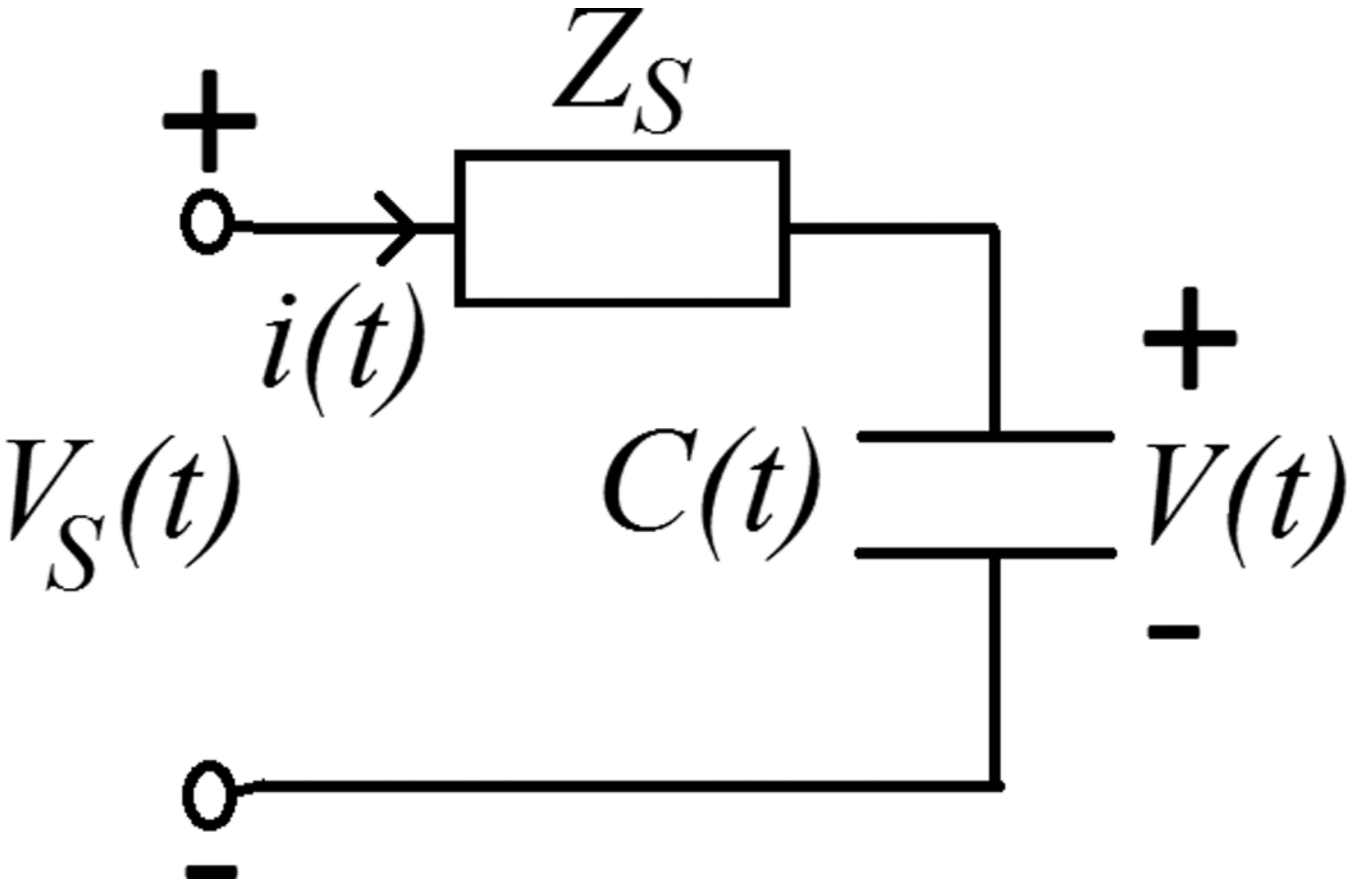


**Fig. 8.**
Resulting electrical circuit with the addition of series impedance to the CMUT capacitance.

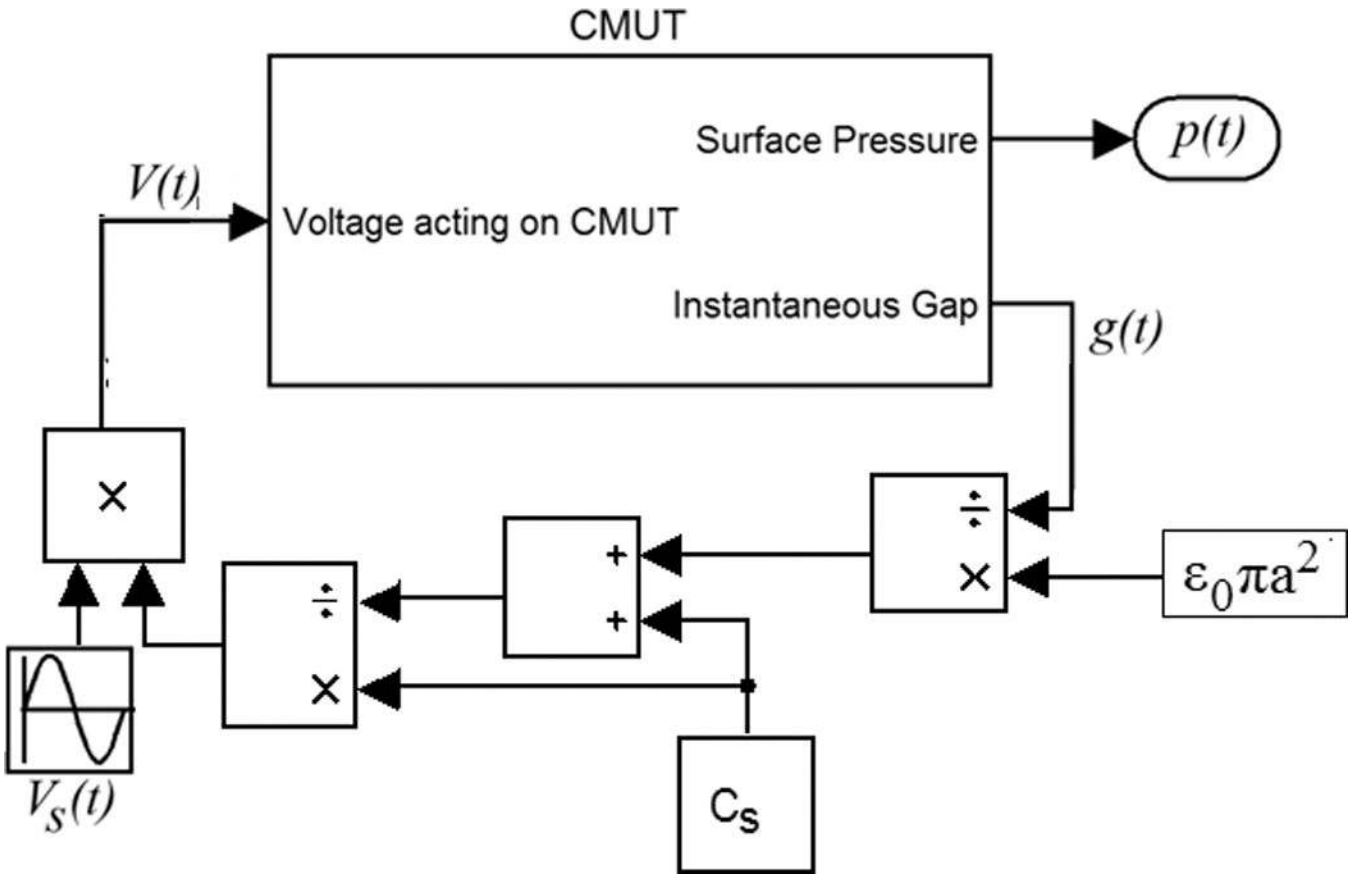


**Fig. 9.**
The SIMULINK model with addition of a series feedback capacitor $C_s$

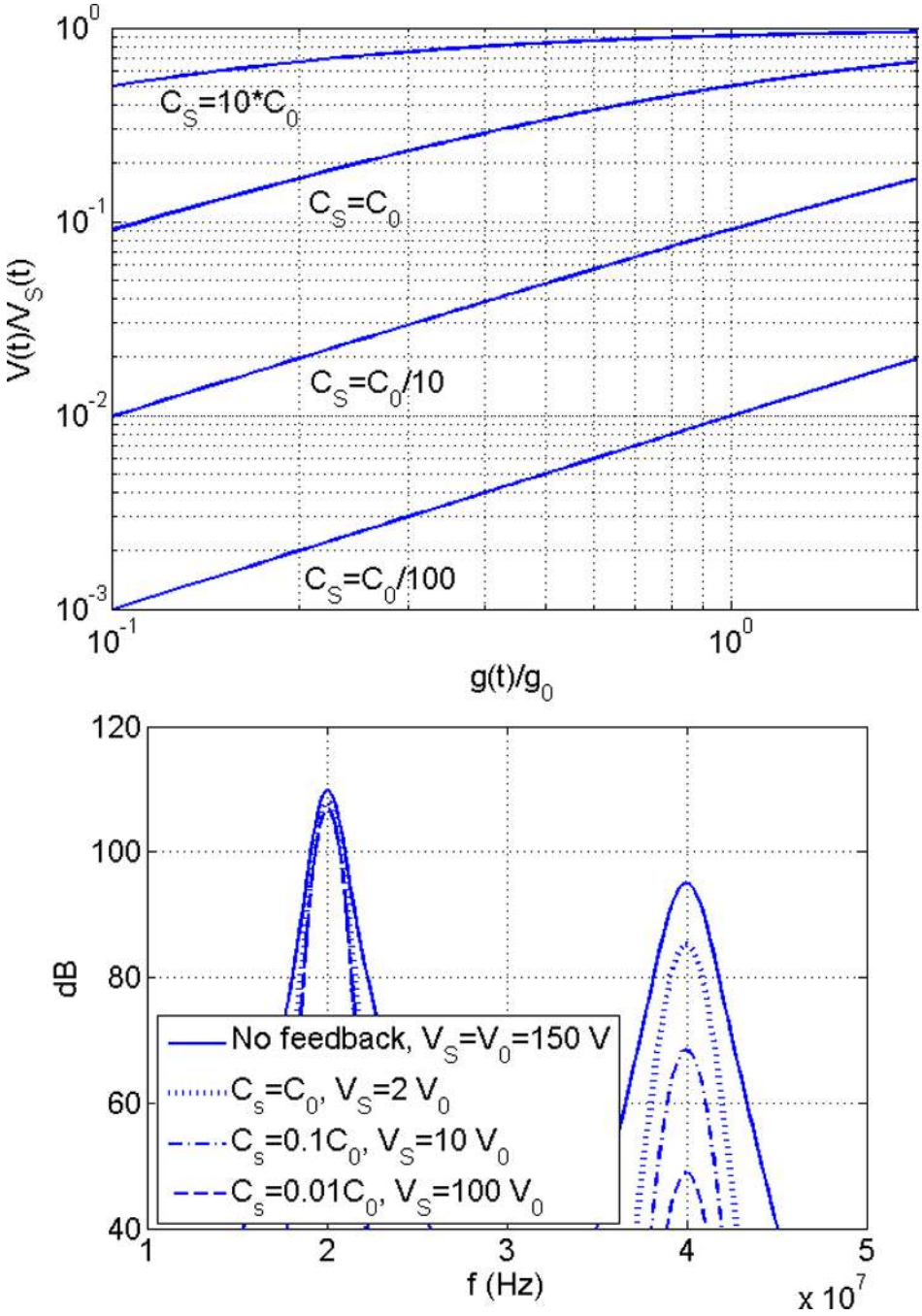


**Fig. 10.**

Top: Voltage acting on the transducer as a function of input voltage and instantaneous gap for different feedback capacitor values. Bottom: 20 MHz and 40 MHz components of the transmitted surface pressure for different series capacitor values and input signal amplitudes where the CMUT is excited at 10 MHz

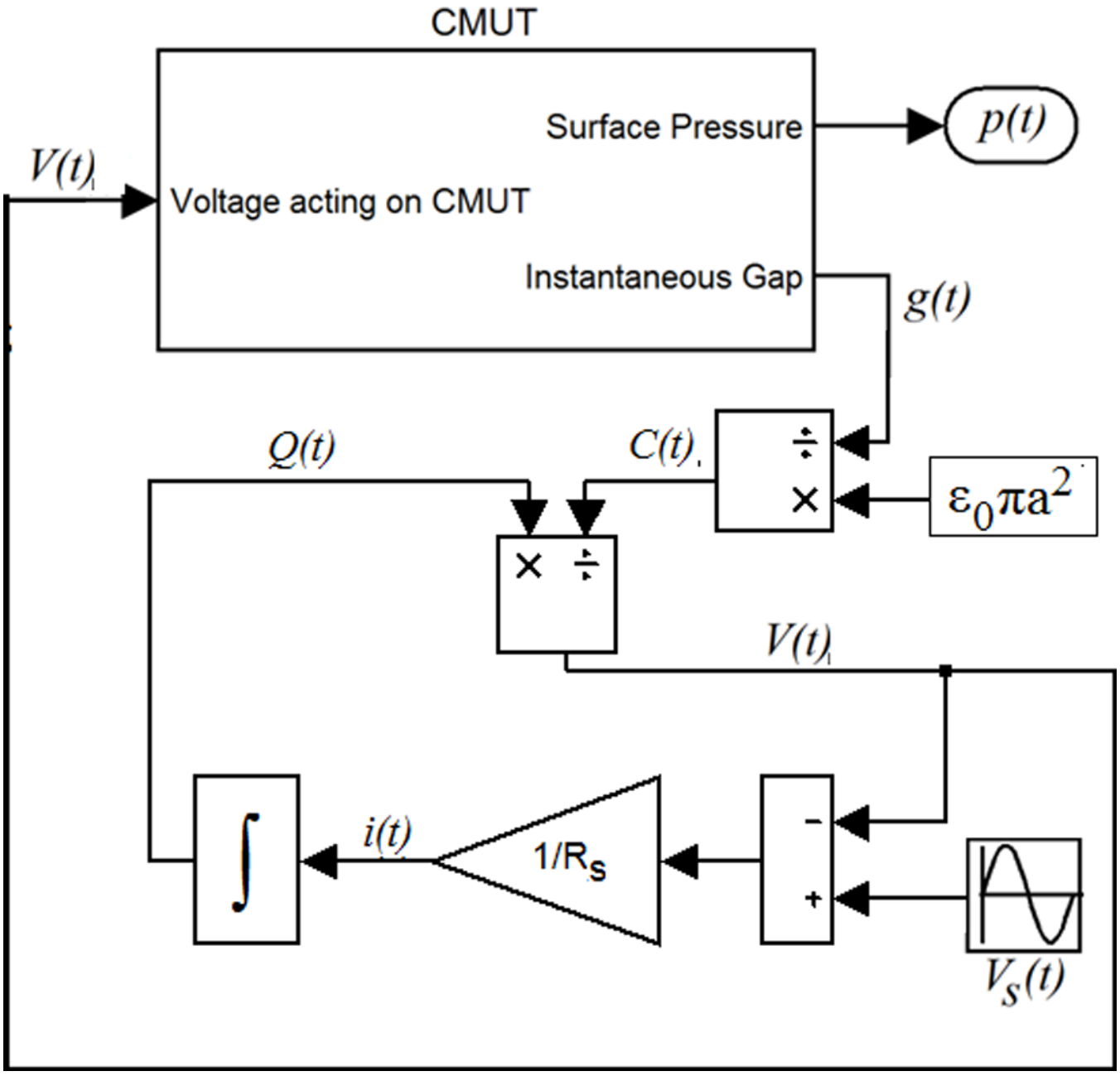


**Fig. 11.**
The SIMULINK model with addition of a series feedback resistor $R_S$

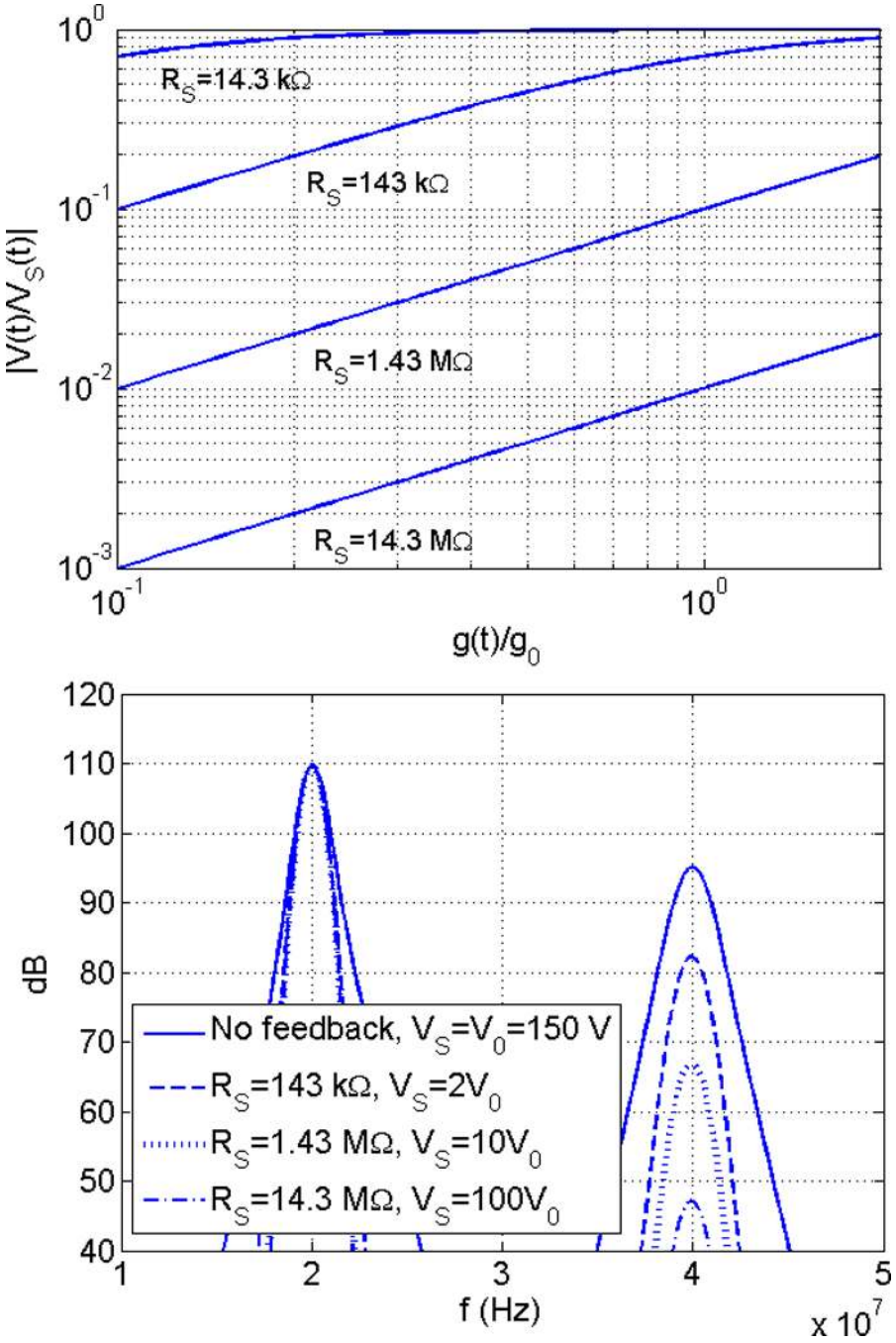


**Fig. 12.**

Top: Voltage acting on the transducer at 10 MHz as a function of input voltage and instantaneous gap for different feedback resistor values. Bottom: 20 MHz and 40 MHz components of the transmitted surface pressure for different series resistor values and input signal amplitudes where the CMUT is excited at 10 MHz

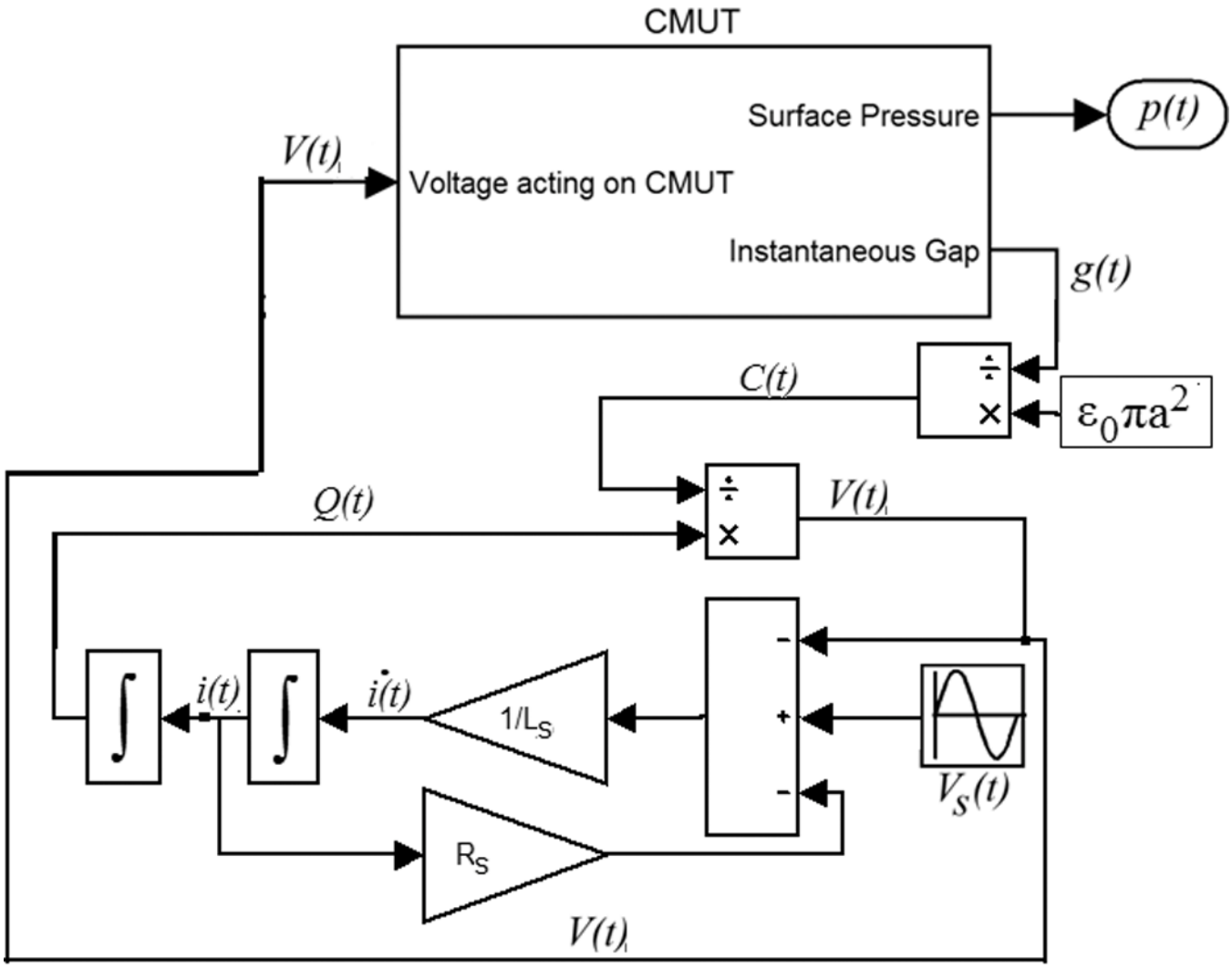


**Fig. 13.**
The SIMULINK model with addition of a series feedback resistor inductor pair

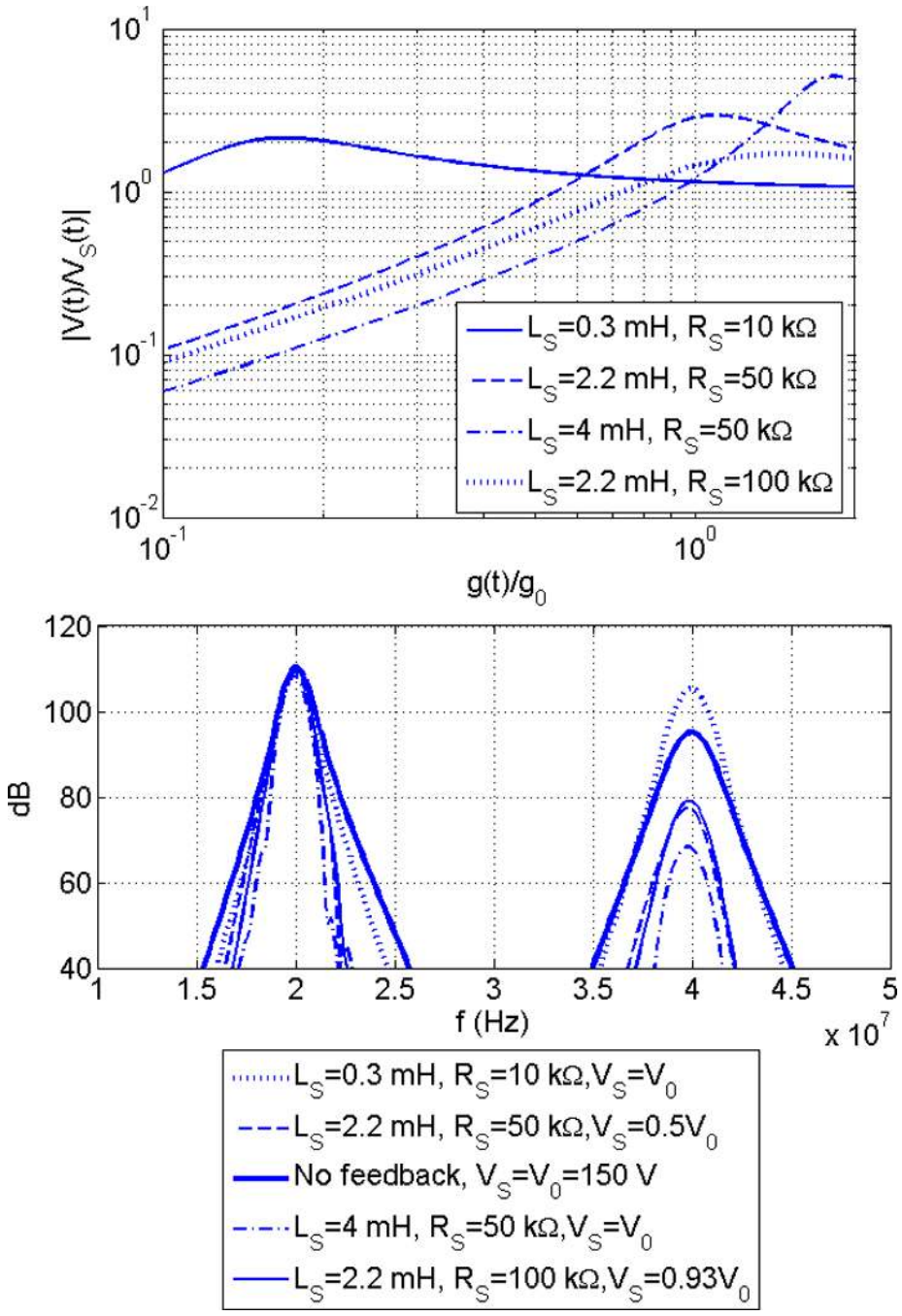


**Fig. 14.**

Top: Voltage acting on the transducer at 10 MHz as a function of input voltage and instantaneous gap for different feedback resistor and inductor values. Bottom: 20 MHz and 40 MHz components of the transmitted surface pressure for different series resistor-inductor pair values and input signal amplitudes where the CMUT is excited at 10 MHz

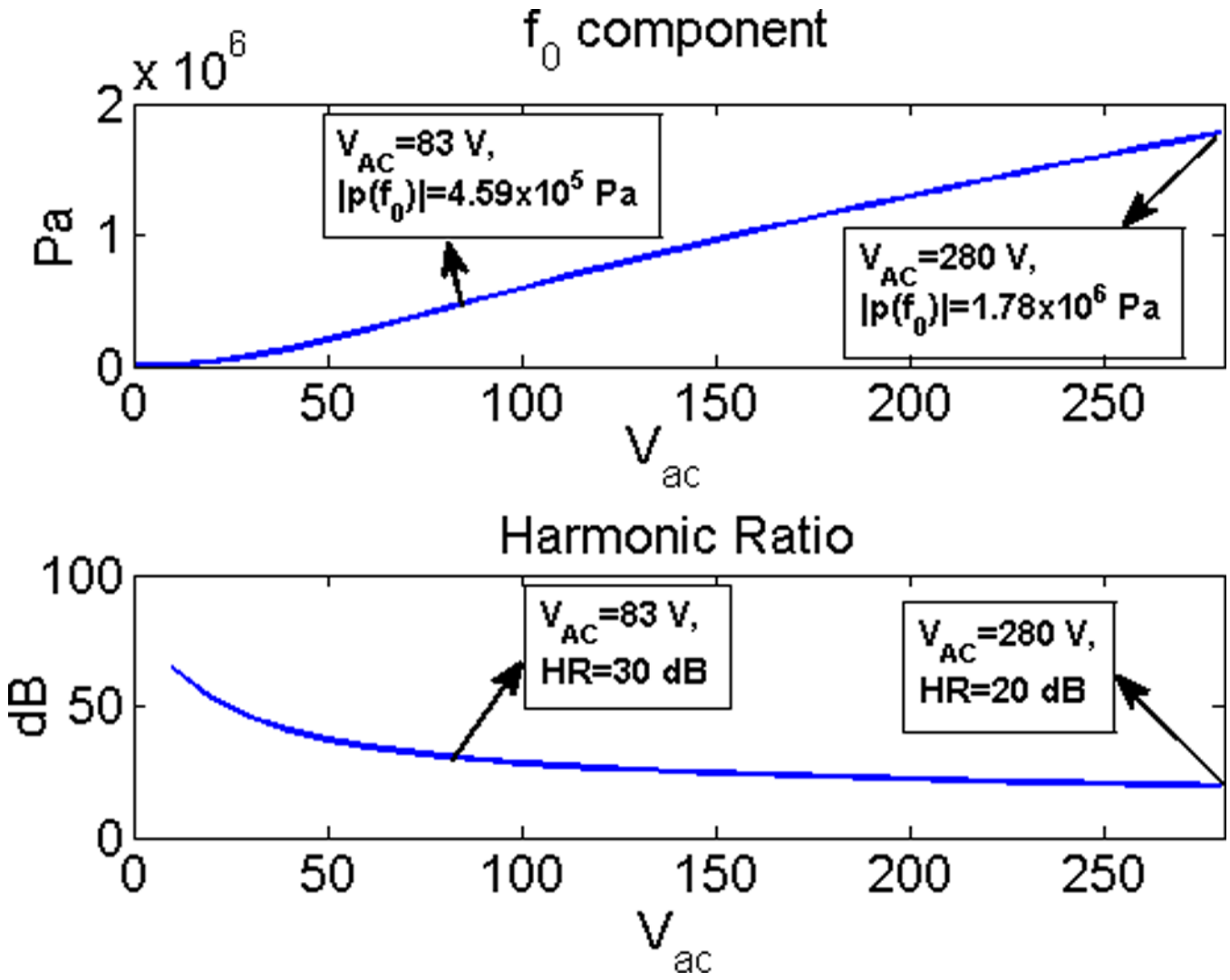


**Fig. 15.**

Top: Magnitude of the $f_0$=20 MHz component of the generated average surface pressure as a function of input signal amplitude at 10 MHz without DC bias with series resistor-inductor pair with values of $R_S$=50 kΩ and $L_S$=2.2 mH. Bottom: Ratio of the magnitudes of 20 MHz and 40 MHz components of the generated pressure as a function of input signal amplitude.

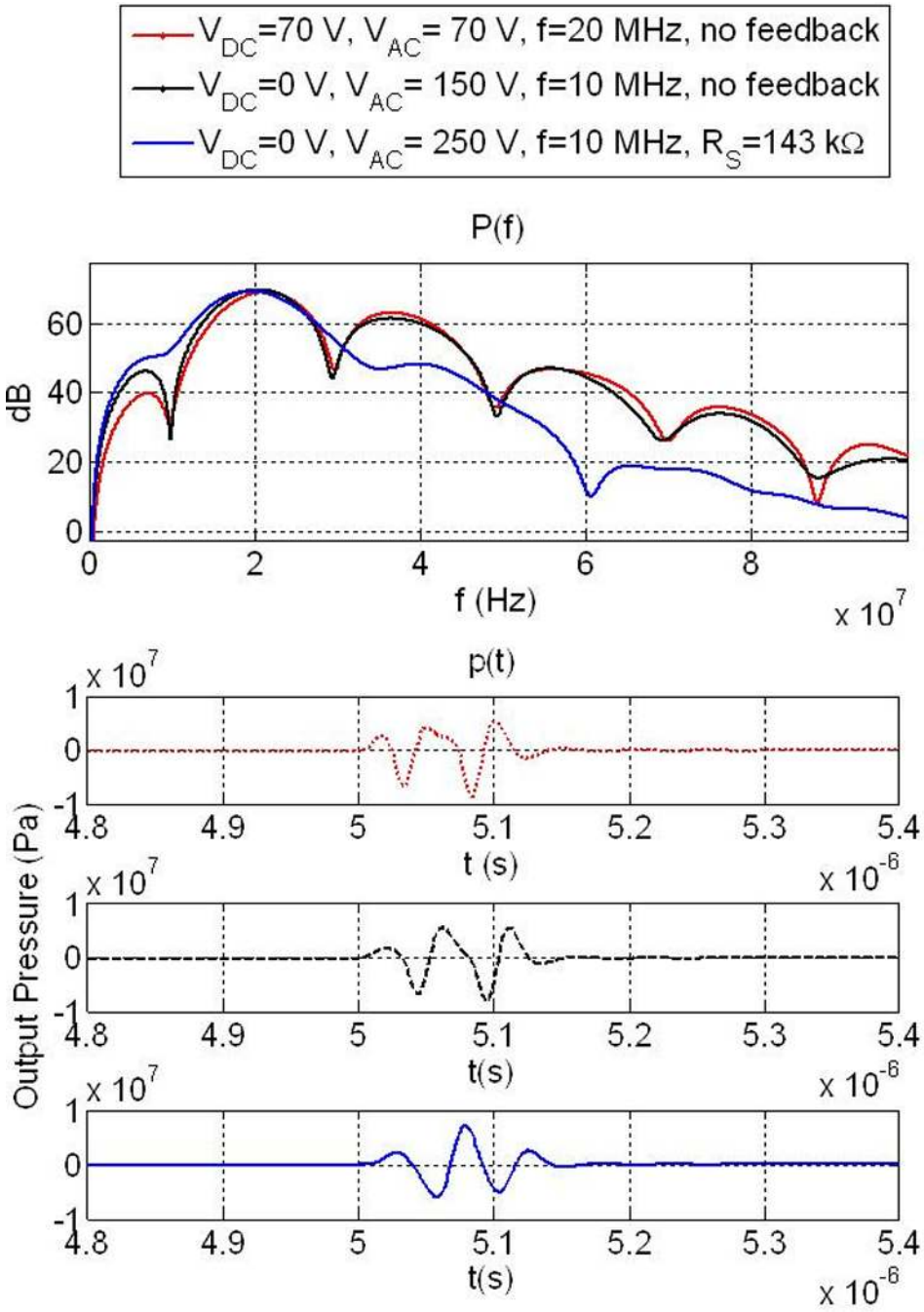


**Fig. 16.**

Top: Spectrum of generated surface pressure for a broadband excitation waveforms. Bottom: Generated surface pressure in time domain for conventional and subharmonic excitation cases with and without feedback.

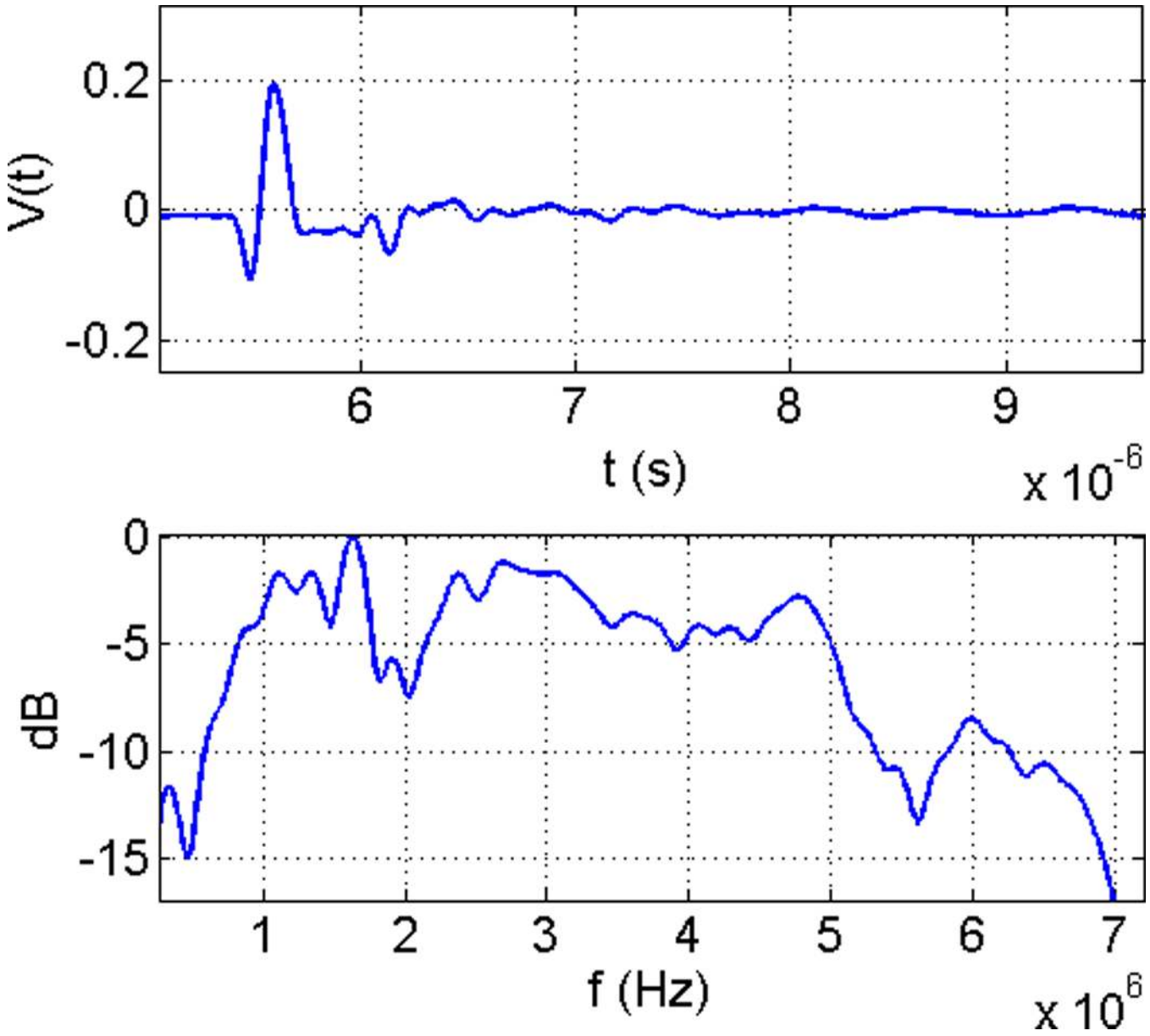


**Fig. 17.**
Pulse-echo response of the CMUT used in the experiment and its frequency spectrum

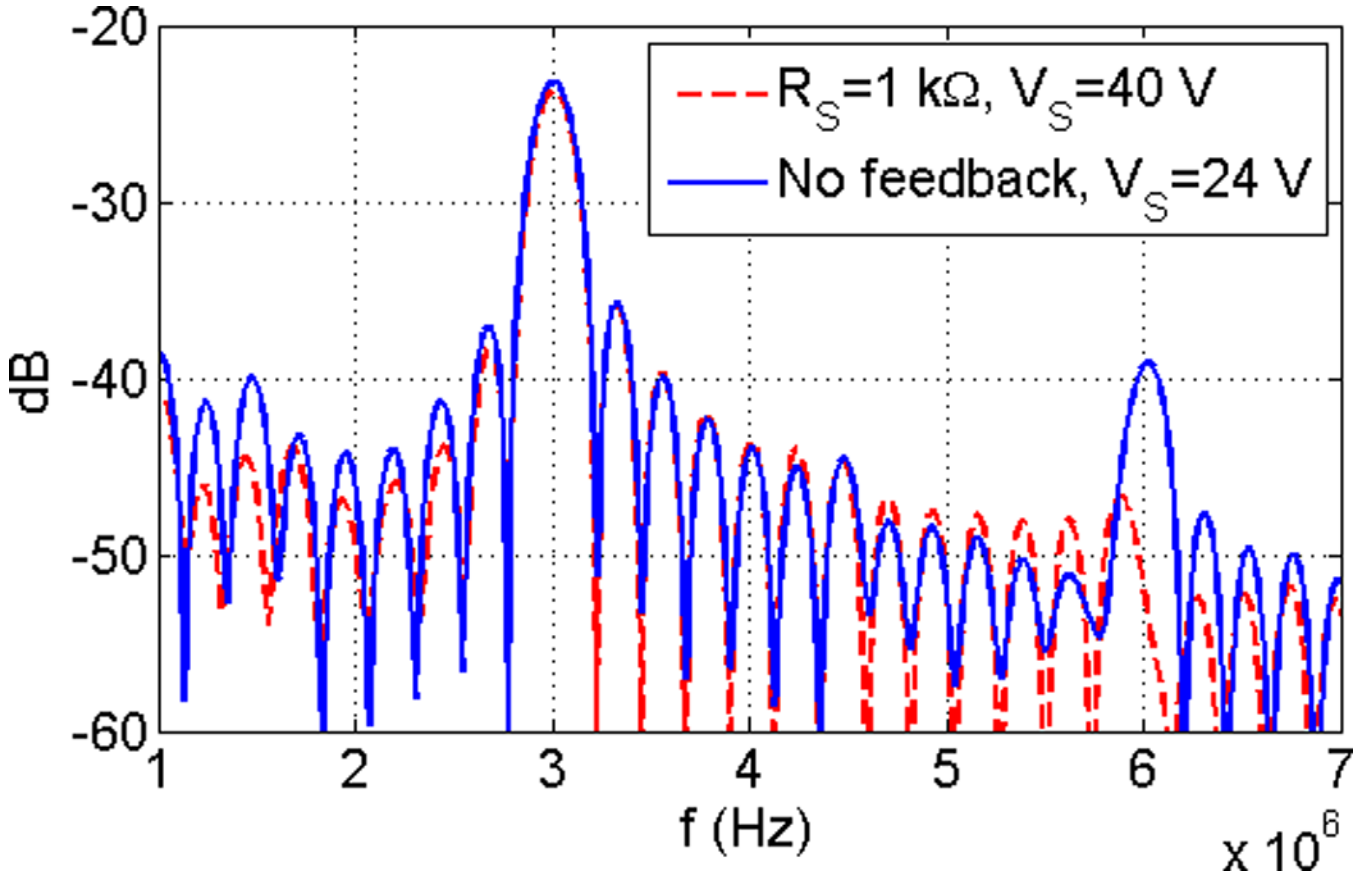


**Fig. 18.**
Frequency spectrum of the received signal with and without resistive feedback where the transducer is excited with a 15 cycle 1.5 MHz tone burst.

**TABLE I**

CMUT Dimensions and Material Properties Used in Simulations

| Property | Value |
|---|---|
| Radius, $a$ | 20 μm |
| Membrane thickness, $t_m$ | 3 μm |
| Initial gap, $g_0$ | 100 nm |
| Membrane density, ρ | 3270 kg/m$^3$ |
| Poisson's ratio of membrane, σ | 0.263 |
| Young's modulus of membrane, $Y_0$ | $3.2 \times 10^{11}$ Pa |
| Density of immersion medium, $\rho_0$ | 1000 kg/m$^3$ |
| Speed of sound in immersion medium, $c$ | 1500 m/s |